2014 ASIA-PACIFIC SOLAR RESEARCH CONFERENCE

Peer Reviewed
2014 Solar Research Conference

Influence of the process parameters on the morphological and electronic properties of liquid phase crystallized silicon films on glass

S. Kühnapfel[1], P. Sonntag[1], B. Rech[1] and D. Amkreutz[1]

[1]*Helmholtz-Zentrum Berlin für Materialien und Energie - Institut für Silizium-Photovoltaik*
Kekuléstr. 5, 12489 Berlin, Germany

E-mail: sven.kuehnapfel@helmholtz-berlin.de

Abstract

The crystallization of thin silicon films directly on glass with a material quality comparable to commercially available multi-crystalline silicon wafers is one of the major goals in thin film technology. In the past the resulting poly-crystalline silicon layers fabricated using the solid phase crystallization (SPC) method suffered from a number of shortcomings such as small grains and a high defect concentration which limited the achievable open circuit voltage to values below 500 mV. We were able to overcome those limitations with liquid phase crystallization (LPC) utilizing a continuous wave diode laser or an electron beam. LPC results in poly-Si on glass with randomly oriented grains up to cm in length and mm in width with a very low amount of intra-grain defects. In this work we show how an improved crystallization process in terms of the scanning velocity of the laser, pre-heating of the specimens and the applied laser intensity leads to a changing morphology of the resulting poly-Si layers. Using a well-defined parameter set, we are able to substantially decrease the amount of high angle boundaries which are known from literature to reduce the overall electronic quality and to trigger a preferential surface orientation of {100}. First a-Si:H/c-Si hetero-junction cells fabricated using this advanced crystallization process showed a benefit in open circuit voltage.

1. Introduction

Liquid phase crystallization (LPC) is a promising technology for poly-crystalline silicon (poly-Si) thin film solar cells on foreign substrates (e.g. glass). LPC offers large laterally grown grains of several cm in length and a few mm in width (Amkreutz et al., 2014), (Haschke et al., 2014), (Eggleston et al., 2012). Similar to multi-crystalline wafers, the quality of LPC material is governed by the grain size, the nature of the resulting grain boundaries, intra-grain defects and impurities. Various studies (Garg et al., 1989), (Tsurekawa et al., 2005), (Seifert et al., 2011), (Wang et al., 1999), (Chen et al., 2004) have shown the influence of the grain size and the nature of the grain boundaries on the electrical properties of the absorber. It was shown that grains featuring a {001} surface inhibit the lowest defect density in terms of grain boundaries, e.g. twins (Cullis et al., 1984), (Nagashio and Kuribayashi, 2005). Moreover, best results for light-trapping concepts based on random pyramid etching (Angermann et al., 2008) are achieved on {001} surfaces. In addition, the resulting {111} facets are known to form a well passivated a-Si:H/c-Si interface. In this work we investigated the formation of preferential grain growth during laser crystallization using a line-shaped continuous wave (cw) laser beam.

2. Experimental

All samples were prepared on 1.1 mm thick Corning Eagle XG glass substrates with a size of 5 × 5 cm^2. The substrates were cleaned with a heated alkaline cleaning agent in an ultrasonic bath. After drying the substrates with nitrogen, a reactively sputtered SiO_2 diffusion barrier of 200 nm thickness was deposited. The 10 µm thick silicon absorber was deposited using

high-rate electron beam evaporation (Sontheimer et al., 2009) at 600 °C and a rate of 300 nm·min^{-1}. As a dopant source served a 5 nm thin phosphorous doped ($N_D \sim 10^{19}$ cm^{-3}) silicon layer sputtered on top of the layer stack. The specimens were placed on a moveable sample stage and were pre-heated up to 750 °C in order to reduce thermal stress during crystallization. Crystallization source was a line-shaped continuous wave laser beam from Lissotschenko Mikrooptik (LIMO) GmbH with a center wavelength of 808 nm, a top-hat profile with a length of 31 mm and a gaussian profile across its width of 0.177 mm (FWHM). The characterization of the resulting absorbers was carried out using visual evaluation, electron backscatter diffraction (EBSD) and X-ray diffraction (XRD). In addition, a-Si:H/c-Si hetero-junction solar cells were fabricated using the contact system described in (J. Haschke et al., 2013). The cell performance was evaluated with suns-V_{OC}.

3. Results and discussion

3.1. Process window

The temperature of the sample stage ($T_{sub.}$), the deposited energy ($E_{F.}$) and the scanning velocity (v_{scan}) were varied in order to identify the different crystallization regimes. In figure 1(a) the crystallization range for samples placed on a heated sample stage with a temperature of $T_{sub.}$ = 700 °C is shown. However, the range is also representative for other pre-heating temperatures as a $\Delta T_{sub.}$ of +/− 100 °C results in a parallel displacement of the measurement curves of approximately −/+ 0.1 J·mm^{-2} [indicated by the double headed arrow in Fig. 1(a)]. The deposited energy density, $E_{F.}$, is depicted as a function of the scanning velocity, v_{scan}. The circles indicate the transition from as-deposited nanocrystalline to small grained poly-Si [exemplarily shown in Fig. 1(b)]. The triangles and squares outline the parameter space where elongated large poly-Si films are obtained [see Fig. 1(c)]. As shown in the graph, the applied energy density decreases with increasing scanning speed. For small scanning velocities ($v_{scan} < 3$ mm/s) a large amount of heat is transferred to the substrate. Thus, below the critical value of 1 mm/s a partial melting of the substrate is observed. This is noticeable by a wave structure at the contact area between the silicon-substrate interface as shown in figure 1(e). On the other hand, for very high velocities most of the introduced heat remains in the silicon resulting in a planar substrate.

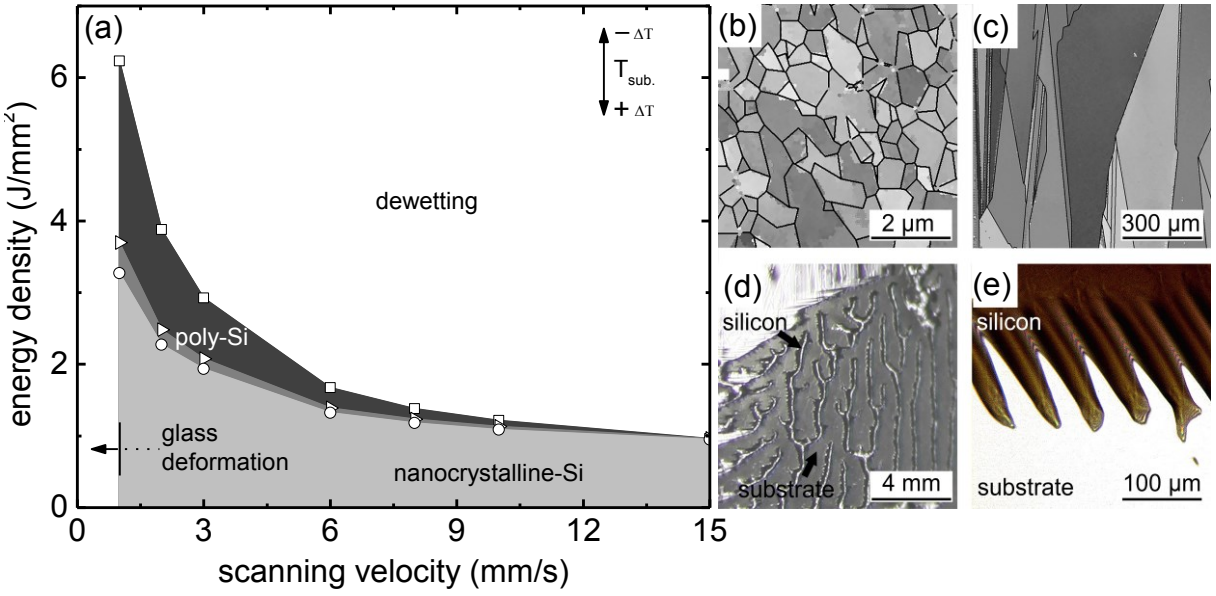

Fig. 1 Phase diagram for the crystallization of 10 µm thick silicon on Corning Eagle XG substrates with a 200 nm SiO_2 diffusion barrier.

The squares in figure 1(a) mark the maximum energy density for lateral grain growth. Above this level the silicon melt starts to partially converge into a branching structure as shown in figure 1(d). This dewetting effect becomes increasingly dominant as the laser intensity is raised. Noticeable in figure 1(a) is that the working range at low scanning velocities turns out to be significantly larger than for fast scanning velocities. While at 2 mm/s a range of almost 14 J·mm^{-2} leads to lateral grain growth at 10 mm/s only a variation of 0.1 J·mm^{-2} decides whether a layer is crystallized or dewetting occurs. At 15 mm/s and beyond, the working range for lateral grain growth disappears. Thus a reproducible stable region is no longer present and a dewetting of the silicon layer is usually observed.

3.2. Absorber morphology

Studies on the growth behavior were performed on samples that were crystalized at v_{scan} = 3 mm/s and $T_{sub.}$ = 700 °C. Those parameters were chosen because they offer a large process window and avoid the deformation of our glass substrates as can be seen in figure 1(a). We investigated the grain orientation as a function of $E_{F.}$. Samples were crystallized at the minimum lateral grain growth threshold (2.08 J·mm^{-2}) and the maximum lateral grain growth threshold just before dewetting occurs (2.92 J·mm^{-2}). Afterwards we evaluated the grain orientation and the boundary angle distribution of approximately 5 – 6 mm² using EBSD. The results are depicted in Fig. 2.

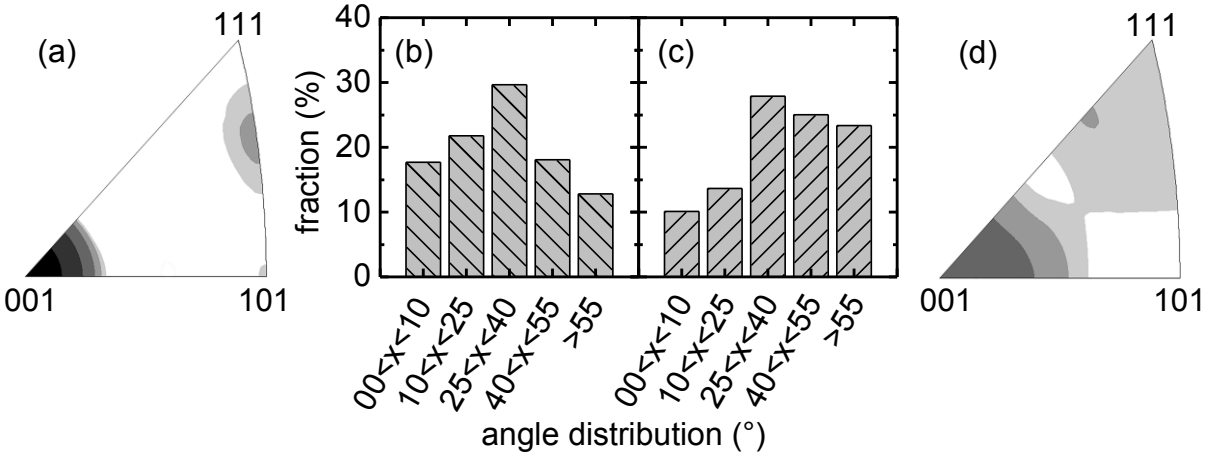

Fig. 2 (a) and (d) show the inverse pole figure of LPC silicon crystallized at a $T_{sub.}$ = 700 °C, v_{scan} = 3 mm/s at the minimum and maximum lateral grain growth threshold, respectively. In (b) and (c) the corresponding boundary angle distributions are depicted.

A clear correlation is observed between the applied $E_{F.}$ and the resulting grain orientation. At an energy density of 2.08 J·mm^{-2} [Fig. 2(a)] we observed a well pronounced {001} orientation for the surface normal. Only a small amount of grains had a surface orientation somewhere between {111} and {101} which in most cases could be attributed to twin boundaries. At an energy density of 2.92 J·mm^{-2} [Fig. 2(d)], which was close to the dewetting threshold, the amount of {001} oriented grains for the surface normal decreased. Instead the amount of grains twisting towards {111} orientation increased. Comparing the angle distribution of samples crystallized at the lowest lateral grain growth threshold [Fig. 2(b)] with samples crystallized close to the dewetting threshold [Fig. 2(c)] shows a clear reduction in high angle boundaries. Grain boundaries with angles from 0 ° – 25 ° occur twice as often at low $E_{F.}$. In return boundary angles above 40 ° are strongly reduced.

We performed additional XRD measurements in order to investigate larger absorber areas to confirm the EBSD findings. The maximum intensities of different lattice plains deduced by integration of the corresponding pole figure are shown in table 1. Specimens crystallized at low $E_{F.}$ exhibit a well pronounced {100} orientation with 35000 counts. In comparison, the intensity of the other investigated lattice planes is more than one magnitude lower. For samples crystallized at an energy density close to the dewetting threshold the preferential grain orientation is lost. The signal strength of {111}, {311} and {400} are similar, only the {220} orientation remains less prevalent.

Table 1. shows the results of the angle dispersive XRD measurements. Depicted are the maximum intensities of the {111}, {220}, {311} and {400} reflections for different crystallization intensities.

Lattice plane	E_{F_low} (counts/s)	E_{F_high} (counts/s)
{111}	160	4500
{220}	10	700
{311}	1200	2140
{400}	35000	4280

3.3. Devices characterization

In order to investigate the electrical properties of our differently crystallized absorber layers hetero junction solar cells with a single sided contact system, extensively described in (J. Haschke et al., 2013), have been fabricated. Suns-V_{OC} measurements have been used to evaluate the open-circuit voltage (V_{OC}) and the pseudo Fill Factor (pFF). The results are depicted in Fig. 3.

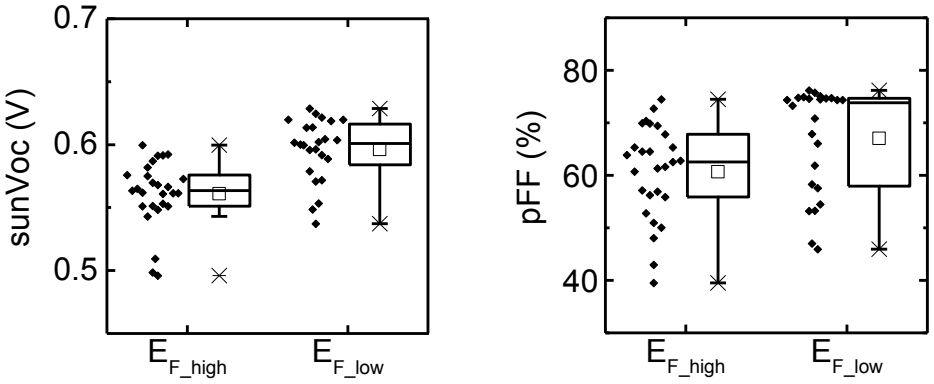

Fig. 3 shows the results of our solar cells measured with suns-V_{OC}

In general, the open circuit voltage is commonly used as an indicator of the material quality (Steffens et al., 2014), (Sontheimer et al., 2013). Despite the strong scattering of the measured sun-V_{OC} values, a clear tendency towards higher voltages can be observed for absorbers that were crystallized at a lower $E_{F.}$. An average increase of 35 mV from 565 mV to 600 mV is observed. These results indicate that a preferential orientation accompanied by a reduction of high angle boundaries results in an increased material quality. Less clearly are the results of

the pFF. In average the pFF increased from 61 % to 74 %. However, the results for both, absorbers crystallized at high and at low $E_{F.}$, are within the uncertainty of the measurement.

4. Conclusion

Using pre-heating temperatures above 650 °C and energy densities within the lateral grain growth regime we were able to successfully crystallize 5 × 5 cm^2 absorbers at scanning velocities between 1 – 15 mm/s without crack formations in our substrates or silicon layers. We were able to show that the process window is significantly larger at low scanning velocities leading to more stable and controllable processes. In addition, subsequent orientation analysis have shown that a preferential grain growth with a high fraction of {001} oriented grains towards the surface normal can be achieved at low v_{scan}, low $E_{F.}$ and high $T_{sub.}$. The preferential orientation of {001} is accompanied by a strong reduction of high angle boundaries as reported in literature before. First devices on such layers have shown that the electronic properties are improved. Especially the V_{OC}, a quality indicator of the material, increases.

Acknowledgements

The authors would like to thank M. Reiche for layer deposition, S. Bischoff for TEM preparation and images, C. Klimm for EBSD measurements and C. Genzel for XRD measurements. This work was supported by the Bundesministerium für Umwelt, Naturschutz und Reaktorsicherheit (BMU) under contract number 41V6178.

References

Amkreutz, D., Haschke, J., Häring, T., Ruske, F., and Rech, B. (2014). Conversion efficiency and process stability improvement of electron beam crystallized thin film silicon solar cells on glass. Sol. Energy Mater. Sol. Cells *123*, 13–16.

Angermann, H., Rappich, J., Korte, L., Sieber, I., Conrad, E., Schmidt, M., Hübener, K., Polte, J., and Hauschild, J. (2008). Wet-chemical passivation of atomically flat and structured silicon substrates for solar cell application. Appl. Surf. Sci. *254*, 3615–3625.

Chen, J., Sekiguchi, T., Yang, D., Yin, F., Kido, K., and Tsurekawa, S. (2004). Electron-beam-induced current study of grain boundaries in multicrystalline silicon. J. Appl. Phys. *96*, 5490–5495.

Cullis, A.G., Chew, N.G., Webber, H.C., and Smith, D.J. (1984). Orientation dependence of high speed silicon crystal growth from the melt. J. Cryst. Growth *68*, 624–638.

Eggleston, B., Varlamov, S., Huang, J., Evans, R., Dore, J., and Green, M.A. (2012). Large Grained, Low Defect Density Polycrystalline Silicon on Glass Substrates by Large-area Diode Laser Crystallisation. MRS Online Proc. Libr. *1426*, 251–256.

Garg, A., Clark, W.A.T., and Hirth, J.P. (1989). Dissociated and faceted large-angle coincident-site-lattice boundaries in silicon. Philos. Mag. A *59*, 479–499.

J. Haschke, L. Jogschies, D. Amkreutz, L. Korte, and B. Rech (2013). Polycrystalline silicon heterojunction thin-film solar cells on glass exhibiting 582 mV open-circuit voltage. Sol. Energy Mater. Sol. Cells *115*, 7–10.

Nagashio, K., and Kuribayashi, K. (2005). Growth mechanism of twin-related and twin-free facet Si dendrites. Acta Mater. *53*, 3021–3029.

Seifert, W., Amkreutz, D., Arguirov, T., Krause, H.M., and Schmidt, M. (2011). Analysis of Electron-Beam Crystallized Large Grained Si Films on Glass Substrate by EBIC, EBSD and PL. Solid State Phenom. *178-179*, 116–121.

Sontheimer, T., Dogan, P., Becker, C., Gall, S., Rech, B., Schubert, U., Young, T., Parlin, S., Keevers, M., and Egan, R. (2009). 6.7% efficient poly-Si thin film mini-modules by high-rate electron-beam evaporation. In 24th European Photovoltaic Solar Energy Conference Proceeding, pp. 2478–2481.

Sontheimer, T., Schnegg, A., Steffens, S., Ruske, F., Amkreutz, D., Lips, K., and Rech, B. (2013). Identification of intra-grain and grain boundary defects in polycrystalline Si thin films by electron paramagnetic resonance. Phys. Status Solidi RRL – Rapid Res. Lett. *7*, 959–962.

Steffens, S., Becker, C., Amkreutz, D., Klossek, A., Kittler, M., Chen, Y.-Y., Schnegg, A., Klingsporn, M., Abou-Ras, D., Lips, K., et al. (2014). Impact of dislocations and dangling bond defects on the electrical performance of crystalline silicon thin films. Appl. Phys. Lett. *105*, 022108.

Tsurekawa, S., Kido, K., and Watanabe, T. (2005). Measurements of potential barrier height of grain boundaries in polycrystalline silicon by Kelvin probe force microscopy. Philos. Mag. Lett. *85*, 41–49.

Wang, Z.-J., Tsurekawa, S., Ikeda, K., Sekiguchi, T., and Watanabe, T. (1999). Relationship between Electrical Activity and Grain Boundary Structural Configuration in Polycrystalline Silicon. Interface Sci. *7*, 197–205.